Materials Letters 257 (2019) 126690

Contents lists available at ScienceDirect

Materials Letters

journal homepage: www.elsevier.com/locate/mlblue

Hot isostatic pressing (HIP) to achieve isotropic microstructure and retain as-built strength in an additive manufacturing titanium alloy (Ti-6Al-4V)

Jake Benzing [a,*], Nik Hrabe [a], Timothy Quinn [a], Ryan White [a], Ross Rentz [a], Magnus Ahlfors [b]

[a] National Institute of Standards and Technology, Applied Chemicals and Materials Division, 325 Broadway, MS-647, Boulder, CO 80305, USA
[b] Quintus Technologies, 8270 Green Meadows Dr. N, Lewis Center, OH 43035, USA

ARTICLE INFO

Article history:
Received 2 July 2019
Received in revised form 23 August 2019
Accepted 15 September 2019
Available online 18 September 2019

Keywords:
Additive manufacturing
Hot isostatic pressing
Microstructure
Recrystallization
Ti-6Al-4V

ABSTRACT

Hot isostatic pressing (HIP) treatments are traditionally used to seal internal porosity, because defects exist in as-built Ti-6Al-4V parts produced by electron-beam melting powder-bed fusion. Standard HIP treatment of Ti-6Al-4V parts results in decreased strength due to coarsening of the microstructure. We present a new HIP strategy with the following steps: hold above the β-transus, rapid quenching, and tempering. This new HIP treatment seals internal porosity, causes a columnar-to-equiaxed transition in morphology of prior-β grains, changes the α lath aspect ratio, removes microstructural heterogeneities and matches the yield and ultimate tensile strength of the as-built condition.

Published by Elsevier B.V.

1. Introduction

Additive manufacturing (AM) of Ti-6Al-4V parts is advantageous for aerospace and biomedical device industries, since this layer-by-layer fabrication method produces complex parts in a fraction of the time with less material waste (as compared to conventional manufacturing methods) [1]. However, electron-beam melting powder-bed fusion (EBM-PBF) of Ti-6Al-4V parts inherently produces elongated prior-β grains and anisotropic mechanical properties [2]. Other defects created during AM include gas pores and lack-of-fusion pores, which are detrimental to fatigue and fracture critical applications [3]. Internal porosity can be sealed during a hot isostatic pressing (HIP) treatment if the compressive stress induced by the HIP pressure is greater than the yield strength of the material at the HIP temperature [4]. All standard HIP treatments [5] of Ti-6Al-4V fall below the β-transus [6] (here defined as a sub-β_{tr} HIP) and typically include slow cooling rates. During these standard sub-β_{tr} HIP treatments, coarsening of grain boundary α and nucleation of coarse intra-granular α laths occurs [7], which results in a decrease in yield and ultimate tensile strength (from a Hall-Petch effect [8]), with respect to the as-built condition. Reduction in strength from a sub-β_{tr} HIP treatment has been reported for many of the common AM processes [9,10]. Also, sub-β_{tr} HIP treatments do not change the elongated prior-β grain morphology [11]. Here, we demonstrate the effectiveness of a new HIP treatment strategy designed to seal internal porosity, produce equiaxed prior-β grains, remove microstructural heterogeneities, and match the strength of the as-built condition. Specifically, the new HIP treatment (subsequently referred to as the super-β_{tr} + temper HIP) includes a rapid quench from above the β-transus and a secondary tempering step.

2. Material and methods

Eighteen Ti-6Al-4V parts (35 mm × 25 mm × 15 mm) were fabricated with an Arcam[1] A1 machine (software version 3.2.132, 60 kV, 50 μm layer thickness, speed factor of 35) and Arcam Ti-6Al-4 V gas-atomized powder (70 μm average diameter). Six parts were left in the as-built condition and six parts were given a standard sub-β_{tr} HIP treatment (900 °C, 100 MPa, 2 h, Ar environment, 12 °C/min heating and cooling rates). The remaining six parts were given a super-β_{tr} + temper HIP treatment (super-β_{tr}: 1050 °C,

[1] Certain commercial software, equipment, instruments or materials are identified in this paper to adequately specify the experimental procedure. Such identification is not intended to imply recommendation or endorsement by the National Institute of Standards and Technology, nor is it intended to imply that the equipment or materials identified are necessarily the best available for the purpose.

* Corresponding author.
E-mail address: jake.benzing@nist.gov (J. Benzing).

https://doi.org/10.1016/j.matlet.2019.126690
0167-577X/Published by Elsevier B.V.

100 MPa, 2 h, Ar environment, 12 °C/min heating rate and approximately 1600 °C/min cooling rate achieved between 1050 °C and 500 °C; temper: 800 °C, 30 MPa, 2 h, Ar environment, 12 °C/min heating and cooling rates). Ten tensile specimens (12.7 mm total length, 3 mm gage length, 2.54 mm gage width, and 1.27 mm thickness) were excised with electrical discharge machining (tensile direction parallel to build direction) and deformed at a strain rate of 1×10^{-3} s^{-1}. An analysis of variance (ANOVA) was completed with InStat software and used to test the null hypotheses that the tensile properties were equal across material conditions; significance is defined as $p < 0.01$.

Samples from each material condition were prepared by mechanical polishing, using 50 nm colloidal silica in the final step. Microstructural characterization and fractography were performed using a field-emission scanning electron microscope (20 kV). Four backscattered electron (BSE) images were captured from random areas (per material condition) for manual α lath thickness measurements (30/image). Samples of each material condition were analyzed for internal porosity with an X-ray computed tomography (CT) machine (160 kV, 10 W, 1 μm voxel size).

3. Results and discussion

Large spherical pores observed in the as-built condition (Fig. 1a) were no longer visible in both the sub-β_{tr} HIP (Fig. 1c) and super-β_{tr} + temper HIP (Fig. 1e) conditions. The as-built and sub-β_{tr} HIP conditions both contained prior-β grains elongated in the build direction (Fig. 1a and c), whereas the prior-β grains in the super-β_{tr} + temper HIP condition (Fig. 1e) were equiaxed (indicating recrystallization). Since elongated prior-β grains lead to anisotropic mechanical properties in EBM-PBF Ti-6Al-4V parts [11], it is reasonable to expect that the super-β_{tr} + temper HIP condition should exhibit isotropic tensile properties.

The microstructures of the as-built and sub-β_{tr} HIP conditions are composed of α laths (dark regions) arranged in a Widmanstätten pattern with β ribs (bright lines) situated between α

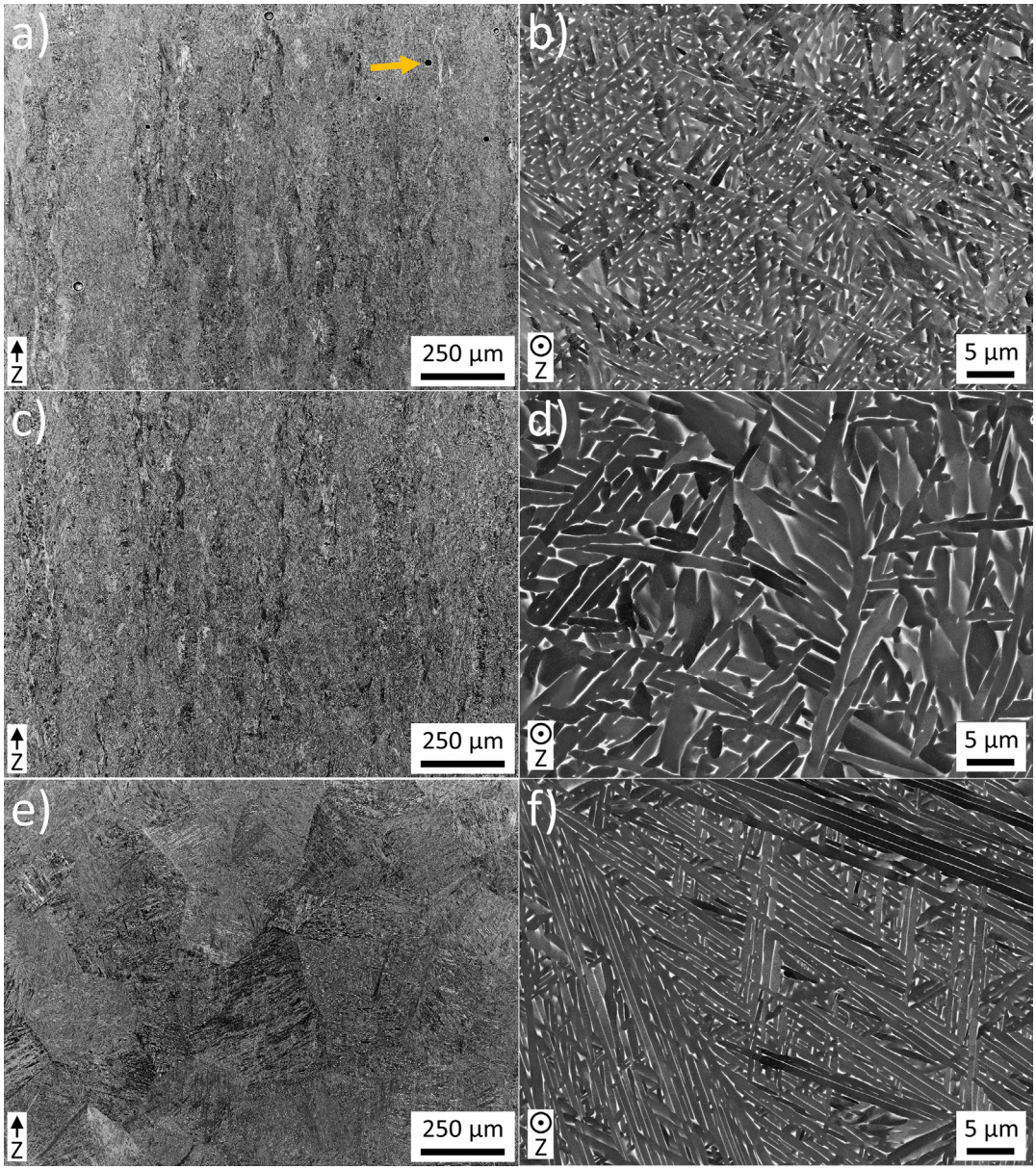

Fig. 1. Backscattered electron images (Z is the build direction) were recorded for the following conditions: a/b) as-built c/d) sub-β_{tr} HIP and e/f) super-β_{tr} + temper HIP. An arrow in a) identifies a gas pore. In the b/d/f) higher magnification images, β is the bright phase and α is the dark phase.

laths, and β spots (bright spots) located within α laths (Fig. 1b and d). The as-built α lath thickness was 1.16 μm ± 0.26 μm. Clear coarsening of α laths occurred after the sub-β_{tr} HIP treatment (Fig. 1d) and produced an α lath thickness of 2.17 μm ± 0.51 μm. After super-β_{tr} + temper HIP treatment, the α lath thickness (1.20 μm ± 0.32 μm) was not significantly different than the as-built condition. The thin α lath thickness is a direct result of applying a sufficiently fast cooling rate when quenching from above the β-transus. Another benefit of the super-β_{tr} + temper HIP treatment was a significant increase in the α lath aspect ratio (another sign of recrystallization) with respect to the as-built condition (lengths of the α laths increased from approximately 5 μm to 50 μm).

X-ray CT revealed spherical gas pores (Fig. 2a), but no flat lack-of-fusion pores in the as-built condition. Porosity comprised 0.21% of the as-built volume, but pores were not detected above the minimum resolvable feature size (approximately 3 μm) by X-ray CT for either of the HIP conditions. However, BSE images of the sub-β_{tr} HIP condition revealed gas pores on the order of 0.9 μm in diameter (Fig. 2c). The small gas pore in Fig. 2c was observed near the center of a group of equiaxed α grains (considered a microstructural heterogeneity in the context of a predominantly Widmanstätten microstructure). These regions of equiaxed α grains were only observed in the sub-β_{tr} HIP condition (in multiple areas across multiple builds), meaning all heterogeneities were erased in the super-β_{tr} + temper HIP treatment.

The HIP treatments did not substantially change the mass fraction for any of the main substitutional elements (Table 1). While the oxygen content increased after both HIP treatments, the resulting increase in strength is estimated to be 11 MPa [13] and thus does not have a strong effect on mechanical properties. Fig. 3a shows a representative engineering stress–strain response for all material conditions. Fractography (Fig. 3b–d) revealed microvoid coalescence on all fracture surfaces in all material conditions. Spherical gas pores were clearly visible on the fracture surface in the as-built condition, while possible remnants of gas pores or other heterogeneities were visible on fracture surfaces for the sub-β_{tr} HIP condition. While the macroscopic features observed on fracture surfaces for the super-β_{tr} + temper HIP condition were more faceted, no gas pores or heterogeneities were observed.

The 0.2% offset yield strength (YS), ultimate tensile strength (UTS), uniform elongation (UE) and total elongation (TE) of the as-built condition were 879 MPa ± 4 MPa, 981 MPa ± 5 MPa, 0.095 ± 0.004 and 0.278 ± 0.028, respectively. The sub-β_{tr} HIP treatment produced a significant reduction in YS (4.7% decrease) and UTS (3.1% decrease), most likely due to coarsening of grain boundary α and nucleation of coarse intra-granular α laths [7]. A significant increase (11%) in TE (Fig. 3f) was noted for the sub-β_{tr} HIP treatment. However, the super-β_{tr} + temper HIP condition produced the greatest average YS and UTS (885 MPa ± 6 MPa and 985 MPa ± 12 MPa). Notably, the YS and UTS of the super-

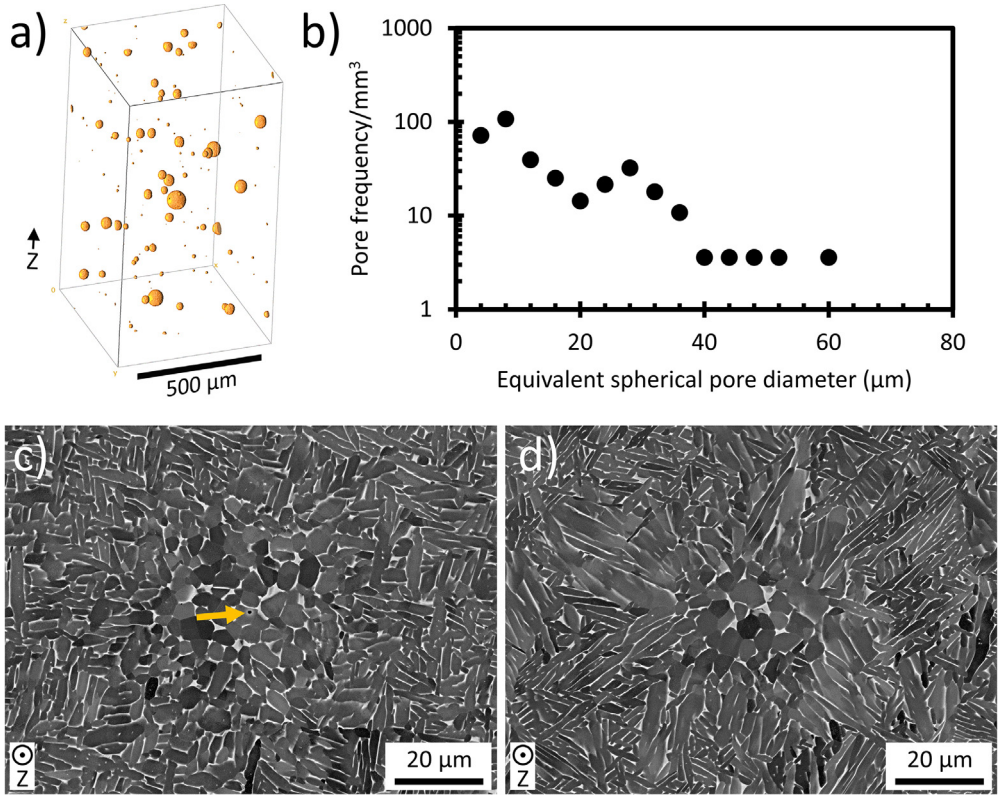

Fig. 2. a) 3-dimensional reconstruction of pore population (X-ray CT) in the as-built condition and the b) corresponding population distribution. c/d) Backscattered electron images recorded from the sub-β_{tr} HIP condition show c) a small gas pore not detected by X-ray CT (see arrow) and c/d) groups of equiaxed α grains.

Table 1
Chemistry of Ti-6Al-4 V parts (% by mass) before and after HIP treatments (measurements conform to ASTM B348-13 [12]).

Material condition	Ti %	Al %	V %	Fe %	O %	C %	N %	H %
As-built	balance	5.82	4.0	0.20	0.100	0.01	0.01	0.001
sub HIP	balance	5.87	4.0	0.20	0.110	0.01	0.01	0.001
super-β + temper HIP	balance	5.78	4.0	0.20	0.115	0.01	0.01	0.012

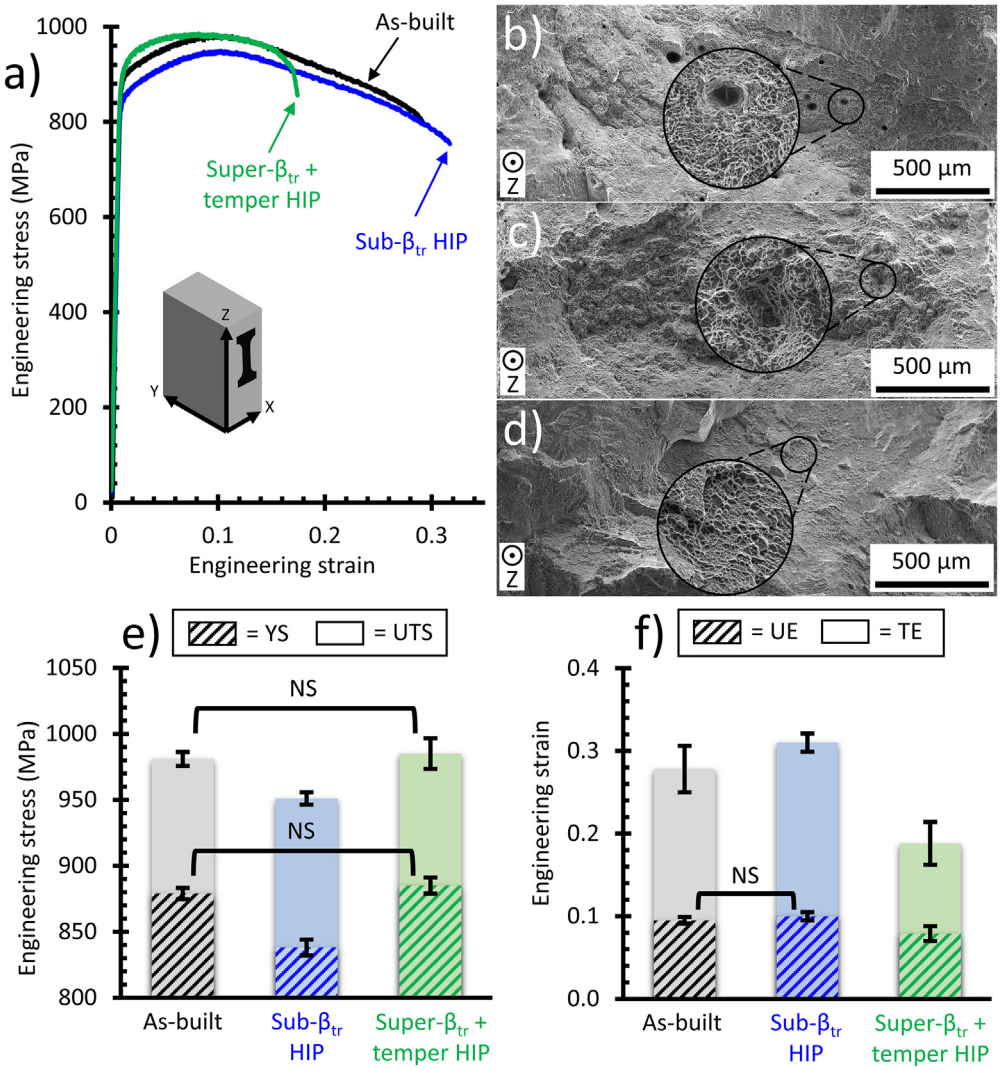

Fig. 3. a) Representative engineering stress–strain curves for all material conditions. Secondary electron images were recorded from the fracture surfaces for the following conditions: b) as-built, c) sub-β_{tr} HIP and d) super-β_{tr} + temper HIP. Bar charts of e/f) tensile properties highlight differences between all conditions (error bars represent one standard deviation). All differences are significant unless noted as non-significant (NS).

β_{tr} + temper HIP condition were not statistically different from the as-built condition.

4. Conclusions

Current limitations of standard sub-β_{tr} HIP treatments include retention of elongated prior-β grain morphologies and a reduction in strength with respect to the as-built condition. Our work shows how a new HIP strategy (rapid quench from above the β-transus and tempering) not only seals porosity, but also maintains α lath thicknesses (1.20 µm ± 0.32 µm), plus yield and ultimate tensile strengths (885 MPa ± 6 MPa and 985 MPa ± 12 MPa) that are not statistically different from the as-built condition. This super-β_{tr} + temper HIP treatment also produces equiaxed prior-β grains, causes an increase in α lath aspect ratio, and removes microstructural heterogeneities.

Declaration of Competing Interest

The authors declare that they have no known competing financial interests or personal relationships that could have appeared to influence the work reported in this paper.

Acknowledgements

This research was performed while Jake Benzing held a National Research Council Postdoctoral Research Associateship at the National Institute of Standards and Technology.

References

[1] B.P. Conner, G.P. Manogharan, A.N. Martof, L.M. Rodomsky, C.M. Rodomsky, D. C. Jordan, J.W. Limperos, Making sense of 3-D printing: creating a map of additive manufacturing products and services, Addit. Manuf. 1 (2014) 64–76, https://doi.org/10.1016/j.addma.2014.08.005.
[2] B.E. Carroll, T.A. Palmer, A.M. Beese, Anisotropic tensile behavior of Ti-6Al-4V components fabricated with directed energy deposition additive manufacturing, Acta Mater. 87 (2015) 309–320, https://doi.org/10.1016/j.actamat.2014.12.054.
[3] N. Hrabe, T. Gnäupel-Herold, T. Quinn, Fatigue properties of a titanium alloy (Ti–6Al–4V) fabricated via electron beam melting (EBM): effects of internal defects and residual stress, Int. J. Fatigue 94 (2017) 202–210, https://doi.org/10.1016/j.ijfatigue.2016.04.022.
[4] J.-M. Franssen, P. Vila Real, Fire Design of Steel Structures, 2nd ed., European Convention for Constructional Steelwork, 2015.
[5] ASTM International (F3001), ASTM F3001 – Standard Specification for Additive Manufacturng Titanium-6 Aluminum-4 Vanadium ELI (Extra Low Interstitial) with Powder Bed Fusion, in: West Conshohocken, PA, 2014. doi: 10.1520/F3001-14.

[6] A.K. Swarnakar, O. Van Der Biest, B. Baufeld, Thermal expansion and lattice parameters of shaped metal deposited Ti-6Al-4V, J. Alloys Compd. 509 (2011) 2723–2728, https://doi.org/10.1016/j.jallcom.2010.12.014.
[7] S.S. Al-Bermani, M.L. Blackmore, W. Zhang, I. Todd, The origin of microstructural diversity, texture, and mechanical properties in electron beam melted Ti-6Al-4V, Metall. Mater. Trans. A Phys. Metall. Mater. Sci. 41 (2010) 3422–3434, https://doi.org/10.1007/s11661-010-0397-x.
[8] Z.C. Cordero, B.E. Knight, C.A. Schuh, Six decades of the Hall-Petch effect – a survey of grain-size strengthening studies on pure metals, Int. Mater. Rev. 61 (2016) 495–512, https://doi.org/10.1080/09506608.2016.1191808.
[9] J.J. Lewandowski, M. Seifi, Metal additive manufacturing: a review of mechanical properties, Annu. Rev. Mater. Res. 46 (2016) 151–186, https://doi.org/10.1146/annurev-matsci-070115-032024.
[10] J.S. Keist, T.A. Palmer, Development of strength-hardness relationships in additively manufactured titanium alloys, Mater. Sci. Eng. A. 693 (2017) 214–224, https://doi.org/10.1016/j.msea.2017.03.102.
[11] J. Wang, H.P. Tang, K. Yang, N. Liu, L. Jia, M. Qian, Selective electron beam manufacturing of Ti-6Al-4V strips: effect of build orientation, columnar grain orientation, and hot isostatic pressing on tensile properties, JOM 70 (2018) 638–643, https://doi.org/10.1007/s11837-018-2794-3.
[12] ASTM International (B348), B348 – Standard Specification for Titanium and Titanium Alloy Bars and Billets, in: West Conshohocken, PA, 2013. doi:10.1520/B0348-13.2.
[13] R. Boyer, E.W. Collings, G. Welsch, Materials Properties Handbook: Titanium Alloys, ASM International, Materials Park, OH, 1994.